CHEMISTRY
A EUROPEAN JOURNAL

DOI: 10.1002/chem.200901987

Binary Au/MWCNT and Ternary Au/ZnO/MWCNT Nanocomposites: Synthesis, Characterisation and Catalytic Performance**

Jayaprakash Khanderi,[a] Rudolf C. Hoffmann,[a] Jörg Engstler,[a] Jörg J. Schneider,*[a] Jürgen Arras,[b] Peter Claus,[b] and Gennady Cherkashinin[c]

Abstract: Gold nanoparticles of 10–24 and 5–8 nm in size were obtained by chemical citrate reduction and UV photoreduction, respectively, on acid-treated multiwalled carbon nanotubes (MWCNTs) and on ZnO/MWCNT composites. The shape and size of the deposited Au nanoparticles were found to be dependent upon the synthetic method used. Single-crystalline, hexagonal gold particles were produced in the case of UV photoreduction on ZnO/MWCNT, whereas spherical Au particles were deposited on MWCNT when the chemical citrate reduction method was used. In the UV photoreduction route, n-doped ZnO serves as the e^- donor, whereas the solvent is the hole trap. All materials were fully characterised by UV/Vis spectroscopy, scanning electron microscopy, transmission electron microscopy, X-ray photoelectron spectroscopy, Raman spectroscopy and BET surface analysis. The catalytic activity of the composites was studied for the selective hydrogenation of α,β-unsaturated carbonyl compound 3,7-dimethyl-2,6-octadienal (citral). The Au/ZnO/MWCNT composite favours the formation of unsaturated alcohols (selectivity = 50% at a citral conversion of 20%) due to the presence of single-crystalline, hexagonal gold particles, whereas saturated aldehyde formation is favoured in the case of the Au/MWCNT nanocomposite that contains spherical gold particles.

Keywords: catalysis · gold · nanocomposites · nanotubes · zinc oxide

Introduction

Prominent examples of the functional properties of multiwalled carbon nanotubes (MWCNTs)[1] include hydrogen storage,[2] chemical and biomedical sensors,[2,3] storage and intercalation of metals such as lithium[4] and catalysis.[5] The attachment of groups to their outer surface is often a key step in the chemical functionalisation of MWCNTs. The covalent linkage of functionalities by fluorination, silylation, lithiation or diazotisation[6] or by converting native surface defects of graphitic structures of CNTs into -COOH or -OH groups by treatment with mineral acids are established techniques of their functionalisation.[7] By attaching inorganic oxides and metal particles to such modified MWCNTs, a class of nanoparticle (0D)–nanotube (1D) hybrid materials becomes accessible. They derive their properties from a combination of the individual properties of the components. Examples are hybrid materials of CNTs with Au,[8,9] Pt or Pd;[9] oxides like TiO_2, ZnO or WO_3;[10] or semiconductors ZnSe, CdS or CdSe.[11] In recent reports, Pt/RuO_2·$x$$H_2O$/CNT and Au,Pt/$SiO_2$/MWCNT have been used as nanocatalysts for fuel cell and oxygen reduction applications.[12,13] We have recently shown that sensing of CO is better with ZnO-functionalised MWCNTs (a ZnO/MWCNT composite) than with MWCNTs alone.[14] When nanoparticle systems are used for catalysis and related applications, irreversible aggregation of active nanocatalysts can be suppressed by limiting their mobility on the CNT surface by means of chemical tethering.[15] This prevents individual nanoparticles from ag-

[a] Dr. J. Khanderi, Dr. R. C. Hoffmann, Dr. J. Engstler, Prof. Dr. J. J. Schneider
Fachbereich Chemie, Anorganische Chemie
Eduard-Zintl-Institut für Anorganische und Physikalische Chemie
Technische Universität Darmstadt
Petersenstrasse 18, 64287 Darmstadt (Germany)
Fax: (+49) 6151-163470
E-mail: joerg.schneider@ac.chemie.tu-darmstadt.de

[b] Dipl.-Ing. J. Arras, Prof. Dr. P. Claus
Fachbereich Chemie, Technische Chemie II
Ernst Berl-Institut für Technische und Makromolekulare Chemie
Technische Universität Darmstadt
Petersenstrasse 20, 64287 Darmstadt (Germany)

[c] Dr. G. Cherkashinin
Fachbereich Material- und Geowissenschaften
Fachgebiet Oberflächenforschung, Technische Universität Darmstadt
Petersenstrasse 23, 64287 Darmstadt (Germany)

[**] MWCNT = Multiwalled carbon nanotube.

Supporting information for this article is available on the WWW under http://dx.doi.org/10.1002/chem.200901987.

glomerating and exposes larger surface areas of the nanoparticle/nanotube interface, thus enhancing the catalytic activity of the particles.

With dimensions below 2 nm, nanoscaled gold typically exhibits quantum-size effects that are attributed to its catalytic reactivity.[16] In addition, the strong interaction of gold nanoparticles with the support leads to a reactive interface region as an active site for catalysis. In addition, the individual shape and morphology of the gold nanoparticles has an important influence on its catalytic activity and selectivity.[17–21] Au nanoparticles supported on TiO_2, ZrO_2, ZnO, Fe_2O_3 and SiO_2 have been used for low-temperature CO oxidation,[18] hydrogenation[19–21] as well as for oxidation of hydrocarbons[18] and so forth. Supported nanostructured gold catalysts show a high selectivity towards hydrogenation of C=O bonds in the presence of double bonds during the conversion of unsaturated aldehyde or ketones to unsaturated alcohols.[19–21] However, studying the direct influence of the support on Au nanoparticles in binary versus ternary composites has, to the best of our knowledge, not been reported.

Herein we present our studies towards the preparation, complete characterisation and catalytic performance of an Au/MWCNT nanoparticle binary composite and an Au/ZnO/MWCNT ternary composite. We studied the latter for whether nanoscale ZnO can 1) serve as a photoactive reduction equivalent to form Au nanoparticles by means of UV decomposition and reduction of Au^{III} salt and 2) serve as a support to these Au nanoparticles. Moreover we studied catalytic hydrogenation test reactions of the α,β-unsaturated aldehyde 3,7-dimethyl-2,6-octadienal (citral) on these new binary and ternary composite nanocatalysts.

Results and Discussion

The generation and deposition of gold nanoparticles on MWCNTs and on the ZnO/MWCNT composite was performed by means of UV irradiation of an alcoholic solution of Au^{III}.[22] This method is able to eliminate any high-temperature calcination/H_2 reduction post-synthesis treatment that is necessary with conventional reduction methods, such as, deposition–precipitation, sol–gel, co-precipitation and incipient wetting.[18] It relies on the fact that noble metal ions of Groups 10 and 11 can be reduced by photoelectrons generated by appropriate semiconductors like ZnO, WO_3 and TiO_2 (see refs. [1–10] in ref. [22]). Herein we study the use of ZnO as a UV-active photoreductant. The active ZnO nanoparticles were synthesised from the single-source molecular precursor $[Zn\{CH_3ONCCH_3COO\}_2]\cdot 2H_2O$ (**1**) by means of impregnation followed by decomposition on the carbon nanotube surface. Precursor **1** decomposes cleanly under moderate conditions via a zinc carbonato intermediate formed in a Beckmann-type decomposition.[23] The thus formed ZnO consists of nanoparticles in the narrow range of 2–10 nm.[14] Scheme 1 shows the synthetic procedure for the synthesis of the Au/ZnO/MWCNT ternary nanocomposite. Synthetic procedures for the other composite materials discussed herein follow a similar route.

The BET surface area of bare MWCNTs, Au/MWCNT and ternary Au/ZnO/MWCNT were determined as 15.76, 23.86 and 19.1 $m^2 g^{-1}$, respectively, by means of nitrogen physisorption. The increase in surface area for the Au/MWCNT composite can be attributed to the fact that the MWCNTs were treated with acid before the deposition of the gold nanoparticles. In the case of the formation of the Au/ZnO/MWCNT composite, the MWCNTs were used as received (no acid treatment). The acid treatment introduces additional coordination sites and end-cap openings, which is believed to cause an increase in the surface area of Au/MWCNT composite.

UV/Vis spectroscopy of the composites: The UV/Vis spectroscopic measurements on suspensions of Au/ZnO (see the Supporting Information), ZnO/MWCNT, Au/MWCNT and

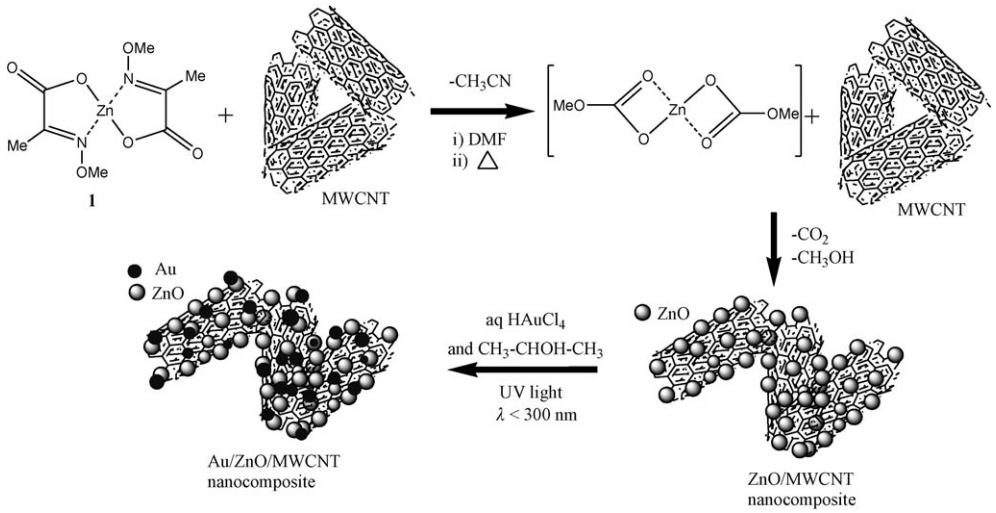

Scheme 1. Decomposition pathway of **1** and deposition route to ZnO/MWCNT and Au/ZnO/MWCNT nanocomposites.

Au/ZnO/MWCNT nanocomposites in ethanol are shown in Figure 1b–e, respectively. The absorption spectrum of gold nanoparticle colloids in Figure 1a is given for comparison. For the gold nanoparticles containing composites, the surface plasmon resonance absorption band at 527 nm (normally observed for gold colloids; Figure 1a) is shifted towards a higher wavelength by approximately (21 ± 2) nm. This redshift in the plasmon band can be attributed to Au particle interactions, to particle size and shape variations of the adsorbed Au nanoparticles on the surface of the MWCNTs or to the formation of ZnO/MWCNT nanocomposites, which changes the local refractive index.[24] The band-gap absorption observed for ZnO in the Au/ZnO/MWCNT composite is shifted towards a higher wavelength by approximately (6 ± 2) nm in comparison with the binary composite ZnO/MWCNT.[14] The ZnO particles in the ZnO/MWCNT composite show a size distribution of 2–10 nm and an absorption of 358 nm[14] (relative to bulk ZnO this a blueshift of (19 ± 2) nm). Such a redshift is also observed for Au deposited on nanoscaled ZnO derived from **1** (Figure 1b). According to theoretical calculations at the quantum mechanical/molecular mechanical (QM/MM) level of Au on ZnO, such results show 1) a reduction of electron density on Au because of its interaction with the surface and 2) that Au^0 has low adsorption energy on ZnO, which allows Au^0 to be partially oxidised to Au^I by transferring electron density to the ZnO conduction band. This explains the redshift observed in the ZnO absorption after Au deposition.[25]

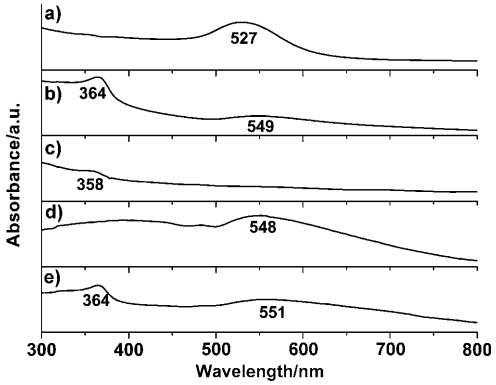

Figure 1. UV/Vis spectra of a) gold nanoparticles obtained by the chemical citrate reduction route; and b) Au/ZnO, c) ZnO/MWCNT, d) Au/MWCNT and e) Au/ZnO/MWCNT nanocomposites obtained by photoreduction. Nanoscaled ZnO is always obtained from thermal decomposition of precursor **1**.[14]

X-ray powder diffraction studies: The structural characteristics of all the composites have been investigated by X-ray powder diffraction (XRD) (Figure 2). XRD analysis of the Au/MWCNT and Au/ZnO/MWCNT nanocomposites indicate the presence of gold in its metallic, zero-valent state in both composites. No signals for other gold species were detected, thus indicating complete reduction of the Au^{III} precursor to Au^0. The remaining peaks can be indexed to either ZnO or graphitic carbon from the MWCNTs.

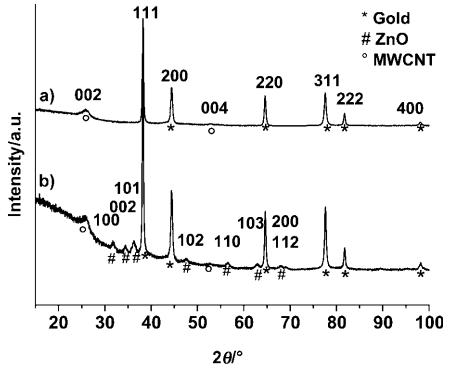

Figure 2. X-ray powder diffraction pattern ($Cu_{K\alpha}$) of a) binary Au/MWCNT and b) ternary Au/ZnO/MWCNT nanocomposite nanocatalysts.

Micro-Raman measurements: Figure 3a–d shows the resonant micro-Raman spectra of bare MWCNTs used as support (trace a), Au/MWCNT (trace b), ZnO/MWCNT (trace c) and the Au-coated ZnO/MWCNT nanocomposite (trace d). The Raman spectra of the MWCNTs and of the nanocomposites show first-order Raman absorptions for the disordered band (D) at 1353 cm^{-1} and the graphene band (G) at 1578 cm^{-1} and second-order Raman signals at 2685 (D*) and 2918 cm^{-1} (D+G) all corresponding to the MWCNT support.[26] In addition, signals corresponding to the E_2 mode at 105 cm^{-1} were observed for the ZnO/MWCNT and Au/ZnO/MWCNT nanocomposites (see inset) indicating that vibrational modes of ZnO are not influenced by the deposition of gold nanoparticles. The shift of the E_2 mode to a higher wavelength relative to bulk ZnO (E_2 resonance mode at 98 cm^{-1}) was assigned to the effect of nanocrystal-

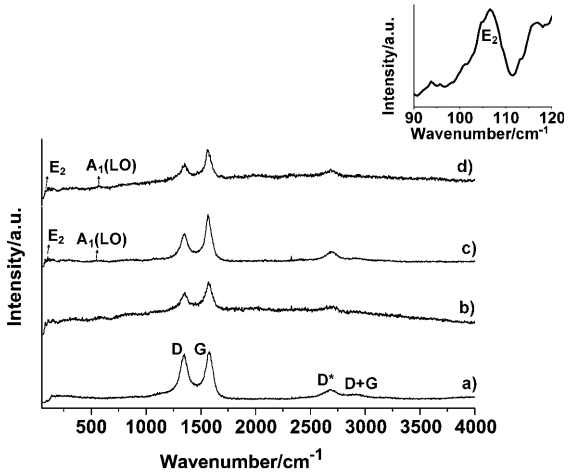

Figure 3. Raman spectra of a) bare MWCNTs, b) Au/MWCNT composite, c) ZnO/MWCNT nanocomposite and d) Au/ZnO/MWCNT nanocomposite. Inset: Magnified view of the E_2 region of the Au/ZnO/MWCNT spectrum.

line ZnO. Similar absorption band shifts have been reported for ZnO nanobelts compared with bulk ZnO.[14,27] The broad absorption at 570–580 cm^{-1} can be assigned to the combined $A_1(LO)$ and $E_1(LO)$ modes.[28] The intensity ratio of I_D/I_G of bare MWCNTs, Au/MWCNT, ZnO/MWCNT and Au/ZnO/MWCNT was calculated to be 0.98, 0.82, 0.65 and 0.75, respectively. The trend shows that after nanoparticle functionalisation of MWCNTs with ZnO and Au the intensity of the defect band decreases. This can be attributed to the fact that defect sites of the MWCNT support act as preferred nucleation sites for the growth of ZnO and Au nanoparticles on the MWCNT surface, thus strongly affecting the defect vibrations of the MWCNTs of the nanocomposites.

X-ray photoelectron spectroscopy (XPS) measurements on Au/MWCNT and Au/ZnO/MWCNT: XPS spectra of Au/MWCNT and Au/ZnO/MWCNT nanocomposites prepared by using UV-light reduction are shown in Figure 4. An XPS survey spectrum (not shown) indicated that gold was in the zero oxidation state. The corresponding binding energies of Au $4f_{5/2}$ and Au $4f_{7/2}$ are 87.8 and 84.1 eV, respectively, for the Au/MWCNT and the Au/ZnO/MWCNT nanocomposites, the same as that observed for bulk gold.[20] The binding energies of Zn $3p_{1/2}$, Zn $3p_{3/2}$ and Zn $2p_{3/2}$ are 92.3, 89.6 and 1022.2 eV, respectively, in good accordance with reported values.[24,29]

The high-resolution XPS spectra of the C 1s and O 1s excitation of Au/MWCNT and Au/ZnO/MWCNT are shown in Figure 5. The MWCNTs were functionalised before the deposition of gold in the case of Au/MWCNT, whereas in the case of gold deposition on ZnO as-received MWCNTs were used. The C 1s spectrum of the MWCNTs shows the graphitic carbon peak at 284.5 eV. A small shoulder, which is more predominant in the case of C 1s of the Au/MWCNT nanocomposite at 286.7 eV indicates -COOH and/or -OH groups generated after functionalisation due to an acid treatment. The O 1s peak has been deconvoluted into two peaks originating at 531.3 eV and a broader one at 532.7–533.3 eV. The first one corresponds to oxygen of ZnO as well as to C=O groups (ca. 531.1 eV) and the second to C–OH groups (532.7–533.3 eV) on the surface of the MWCNTs.[30,31]

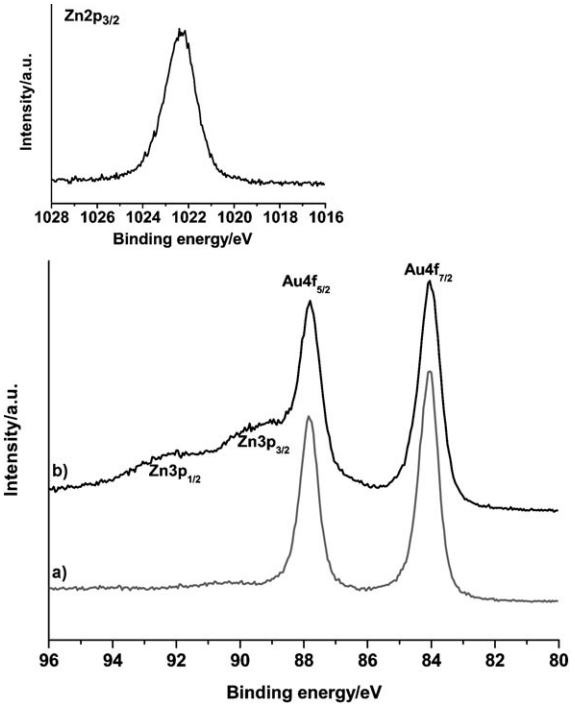

Figure 4. X-ray photoelectron spectra of a) the Au $4f_{5/2}$/Au $4f_{7/2}$ region of gold in the Au/MWCNT nanocomposite and b) the Zn $3p_{1/2}$/Zn $3p_{3/2}$ and Au $4f_{5/2}$/Au $4f_{7/2}$ regions of gold and ZnO for the Au/ZnO/MWCNT nanocomposite. The inset shows the Zn $2p_{3/2}$ trace of the Au/ZnO/MWCNT nanocomposite.

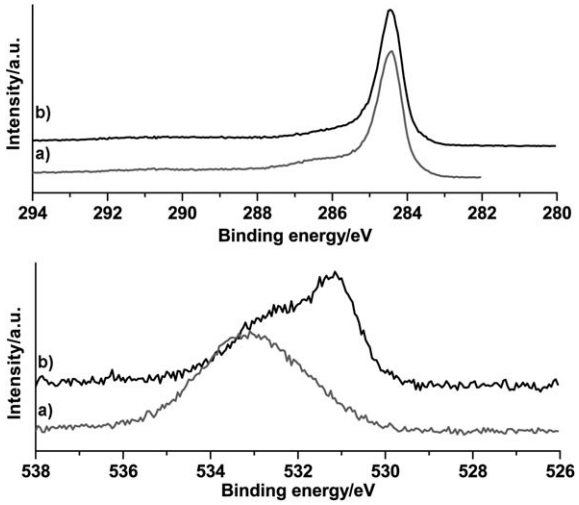

Figure 5. X-ray photoelectron spectrum of the C 1s region (upper traces) and O 1s region (lower traces) in a) Au/MWCNT and b) Au/ZnO/MWCNT nanocomposites.

Scanning electron microscopy (SEM): SEM analysis of the Au/MWCNT binary nanocomposite obtained from the chemical citrate reduction route and of the Au/ZnO/MWCNT ternary nanocomposite obtained by UV photodecomposition are shown in Figure 6. Au particles with a mean diameter of 23.1 nm can be seen in the binary nanocomposite (Figure 6 top). This value is in agreement with an average crystallite size of 24 nm determined from XRD by using the Scherrer equation. The Au particles are present on the surface of the MWCNT in a very dispersed manner. In the case of the Au/ZnO/MWCNT nanocomposite (Figure 6 bottom), the Au particles were generated by UV photodecomposition on the ZnO/MWCNT composite. Although this reduction technique should in principal provide smaller Au particles, only larger aggregates in the range 24–100 nm were detected close to one another on the surface of the MWCNTs. We attribute their size to the formation of Au/ZnO composite particles on the surface of the MWCNT.

Indeed, the UV-photocatalytic reduction of gold chloride needs the presence of a photoactive defect-rich oxide like

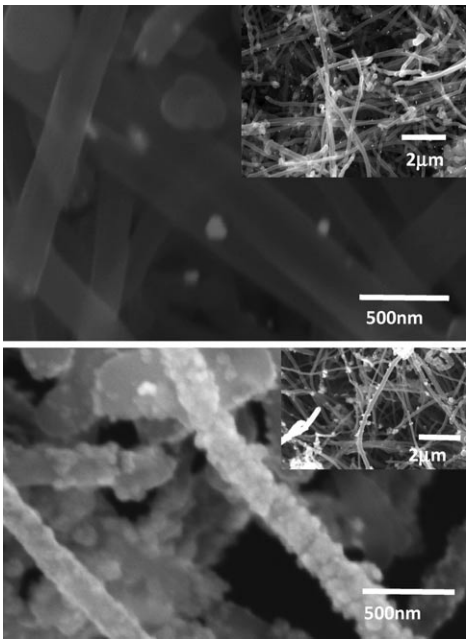

Figure 6. SEM images of Au/MWCNT from the citrate reduction route (top) and Au/ZnO/MWCNT obtained from the UV photoreduction route (bottom). The insets in both cases show an overview of gold nanoparticles and Au/ZnO distributed on the MWCNTs.

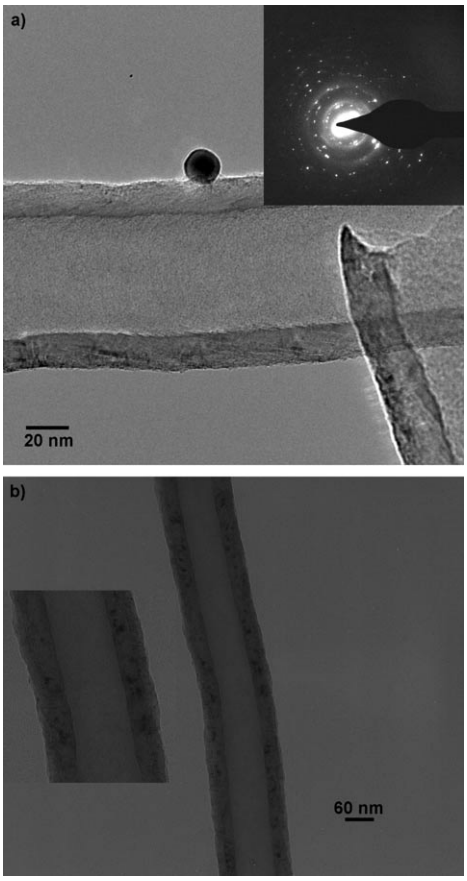

Figure 7. TEM of gold nanoparticles on MWCNTs synthesised by a) the citrate reduction route (inset: the SAED pattern of the gold particle) and b) UV photoreduction of gold chloride. The dark regions indicate a discrete coating of gold particles deposited on the MWCNTs by a UV photoreduction route (inset: a magnified image of the centre part of the CNT).

ZnO to generate electron (e^-)–hole (h^+) pairs. The photogenerated electrons thus initiate the reduction process of the Au^{3+} ions to form zero-valent Au^0 nanoparticles.[22] The solvent isopropanol serves as the hole trap.[22] The Au particles should thus be in close vicinity, or even tethered to the ZnO nanoparticles on top of the MWCNTs. To prove the situation further, we studied their structure by TEM and high-resolution TEM (HRTEM).

Transmission electron microscopy (TEM): First we carried out TEM analysis of gold nanoparticles deposited on MWCNTs by the citrate reduction and UV-light-assisted photoreduction without the photoreductant ZnO (Figure 7a and b, respectively). The gold particles were of a larger size, between 10 and 24 nm, for the citrate reduction route, whereas a discrete coating with small gold nanoparticles (5–8 nm) was observed in the case of the photoreduction method. The unbundled MWCNTs have an absorption band at around 267 nm.[14,32] The result that photoreduction of Au^{III} can indeed already be achieved in the presence of isopropanol as hole scavenger points to the fact that the defect-rich MWCNTs offer photoactive sites for the generation of electron–hole pairs, which serve as a reductant for Au^{III}. However, this effect is much more pronounced when the ZnO/MWCNT composite is used as photoinitiator for the Au nanoparticle deposition and is shown in the TEM analysis of the Au/ZnO/MWCNT nanocomposite (Figure 8). Gold nanoparticles of 2–5 nm are present on the surface of the ZnO and those of 8–10 nm are present on regions of the MWCNT where no ZnO is tethered to the CNT surface (Figure 8a–d, for a detailed TEM analysis of the ZnO/MWCNT composite see ref. [14]). The deposited ZnO comprises slightly elongated particles, and depending on the amount of precursor **1** used, it is possible to load the surface of the MWCNTs accordingly. During the formation of Au nanoparticles on the ZnO/MWCNT composite no change in the morphology of the previously deposited ZnO was observed.

Thus, the noteworthy observations are that 1) the deposition of Au on ZnO is much denser than that on bare, ZnO-free regions of the MWCNTs and 2) the particles are much smaller in the case of Au/ZnO compared with the Au/MWCNT surface regions of the Au/ZnO/MWCNT composite (compare Figure 8a and c). Au nanoparticles are, however, in close contact both with the ZnO nanoparticles and with the MWCNT. This certainly facilitates a larger interface contact, which in turn plays an important role in the catalysis involving gold nanoparticles. Gold particles on ZnO have a hexagonal shape, whereas Au particles on bare MWCNTs are spherical. HRTEM images show [111] facets of Au ($d=0.23$ nm) and [102] facets for ZnO ($d=0.19$ nm) particles. The selected-area electron diffraction (SAED) pat-

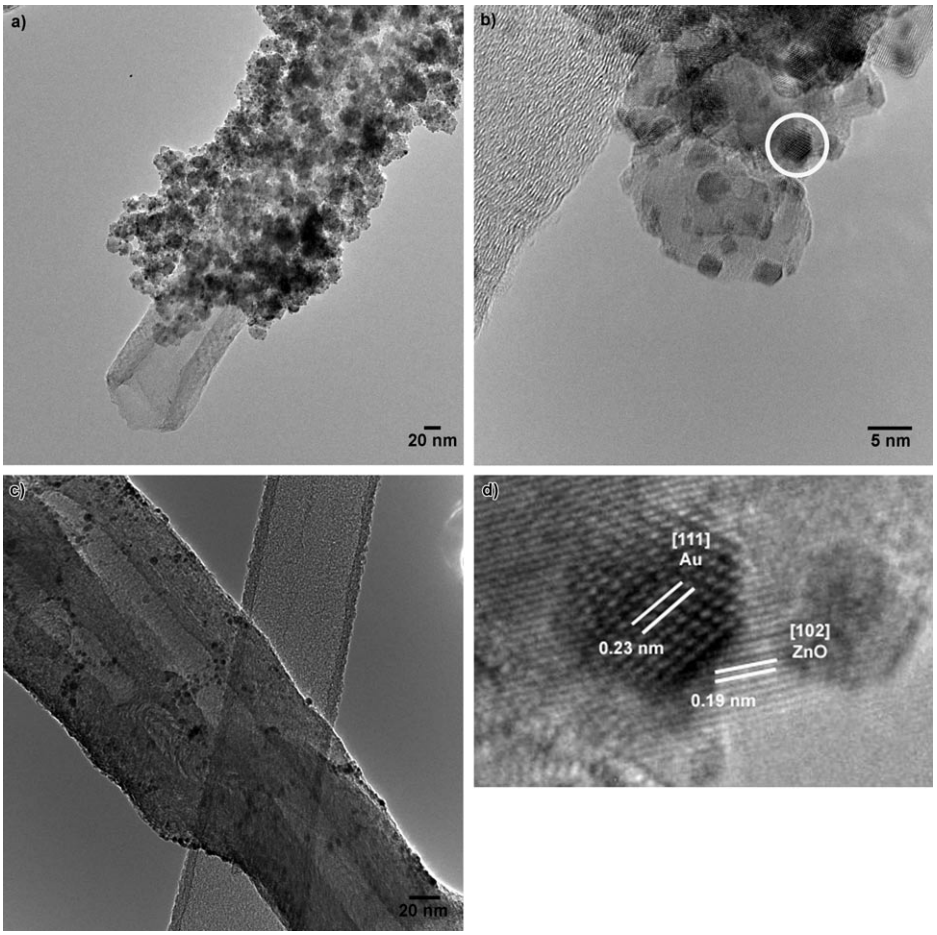

Figure 8. TEM and HRTEM of the Au/ZnO/MWCNT nanocomposite obtained from photoreduction. a) Au/ZnO/MWCNT composite overview; b) as in (a) but at a higher magnification; c) gold nanoparticles deposited on MWCNTs in the areas in which ZnO is seen; d) HRTEM of the interface of Au/ZnO of the marked section in (b).

tern (inset of Figure 8b) proves the highly crystalline nature of the Au/ZnO composite on the surface of the MWCNT.

TEM analysis of the Au/ZnO/MWCNT nanocomposite obtained by means of the chemical citrate reduction route (Figure 9a and b) indicated that gold nanoparticles are preferentially reduced and deposited on the ZnO only. In contrast to the photoreduction technique, the Au particle size is distinctly below 8 nm.

Catalytic activity of Au/MWCNT and Au/ZnO/MWCNT: The Au/MWCNT and Au/ZnO/MWCNT nanocomposites were tested for their catalytic activity and selectivity during the hydrogenation of 3,7-dimethyl-2,6-octadienal (citral), which belongs to a class of α,β-unsaturated aldehydes and has three unsaturated bonds (a conjugated system comprised of C=C and C=O groups as well as an isolated C=C bond). Table 1 gives an overview of the catalytic properties in terms of activity (citral conversion after 360 min) and selectivity to the unsaturated alcohols (geraniol and nerol; UOL) and the saturated aldehyde (citronellal; CAL) for the different composite catalysts with respect to its preparation method, composition and Au particle size and morphology. Note that because of the complex reaction network of citral hydrogenation consisting of competitive and consecutive reactions (e.g., further hydrogenation of UOL and CAL to citronellol and 3,7-dimethyloctanol), the selectivities towards UOL and CAL must be compared at constant conversion.

Table 1 shows that MWCNTs alone are active for hydrogenation, which is accounted for by their surface defect sites producing unknown compounds during the catalytic reaction. It can be further observed that the selectivity to the unsaturated alcohol (UOL) is significantly higher when using the ZnO-modified nanocomposite Au/ZnO/MWCNT, which yields 50% of the desired products. This clearly indicates a correlation between the catalyst performance and the Au nanoparticle shape (single crystalline, hexagonal vs. spherical gold particles for Au/ZnO/MWCNT and Au/MWCNT, respectively) suggesting that control of the intramolecular selectivity (C=O vs. C=C hydrogenation) is structure-sensitive. With regard to the activity of supported gold catalysts during hydrogenation, it must be kept in mind that, besides the support type, a co-operative effect of particle size, degree of particle rounding and portion of multiply twinned particles must be considered as shown in the selective hydrogenation of the simplest α,β-unsaturated aldehyde, acrolein.[17,19] In the present study the catalyst with the largest gold particles (10–24 nm, Au/MWCNT), which are spherical, exhibited the highest activity (Table 1). In the case of oxidic supports, the higher turnover frequency of an Au/TiO_2 catalyst compared with Au/ZrO_2 has been ascribed to the higher degree of rounding of the dominating single-crystalline face-centred cubic (fcc) particles, that is, a higher portion of low-coordinated surface sites.[33] The Au/MWCNT nanocomposite prepared by UV photoreduction displays lower catalytic activity than Au/MWCNT prepared by chemical citrate reduction in accordance with the finding that the nanoparticle morphology of the former is irregular.

Thus, relative to Au/MWCNT, the Au/ZnO interface in Au/ZnO/MWCNT clearly provides interfacial active sites adjacent to the gold particles that can activate the C=O groups of the reactant. This finding indicates that functional-

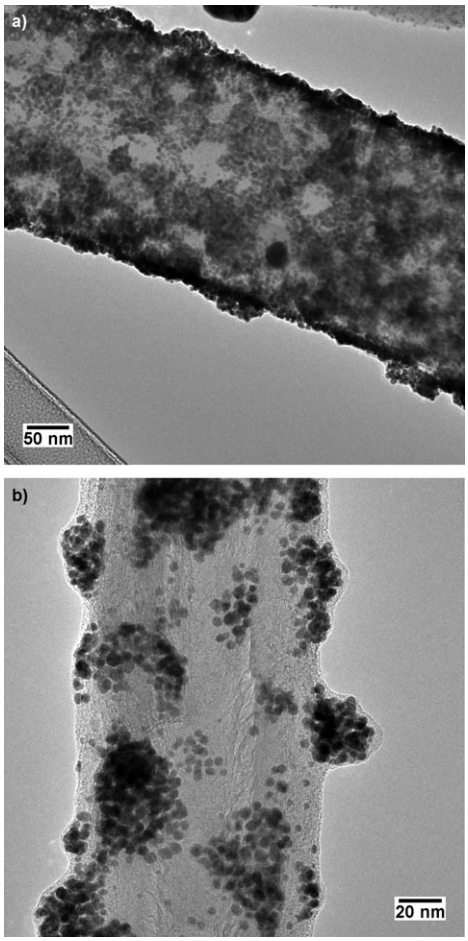

Figure 9. TEM of the Au/ZnO/MWCNT nanocomposite. The Au particles on the ZnO/MWCNT have been synthesised by using the chemical citrate reduction route. a) Overview. b) Higher magnification of deposited Au/ZnO nanoparticle islands.

isation of the MWCNTs with oxides plays a crucial role in the use of these nanocomposites as catalysts.

Conclusion

The synthesis and characterisation of binary and ternary nanocatalysts of the type Au/MWCNT and Au/ZnO/MWCNT has been successfully demonstrated by photoreduction and conventional citrate reduction. The method of deposition of gold nanoparticles has a significant impact on the final size and shape of the gold nanoparticles on the MWCNTs and on ZnO/MWCNT. It was found that nanoscaled ZnO can be used as an effective photoreductant for Au^{III} on MWCNTs. Nevertheless, MWCNTs also offer photoactive sites able to reduce Au^{III} by means of photogenerated electrons. SEM and TEM show that such Au nanoparticles preferentially deposit on ZnO and are 2–5 nm in size, and those deposited on the MWCNT are between 10 and 24 nm. XRD and XPS data indicate that the deposited gold is in a metallic zero-valent state with no other oxidation states of gold present. UV/Vis spectroscopy indicates a redshift in the plasmon band of Au as well as that for Au/ZnO deposited on MWCNT. The results of citral hydrogenation indicate clearly that the presence of ZnO on the MWCNT increases the selectivity towards C=O group hydrogenation due to the presence of single-crystalline, hexagonal gold particles. In contrast, the Au/MWCNT composite, irrespective of the method of synthesis, shows poor selectivity towards the unsaturated alcohols.

Experimental Section

General: MWCNTs with a diameter of 150 nm were purchased from Electrovac, Klosterneuburg, Austria. They were further treated with boiling concentrated HNO_3 for approximately 18 h before the deposition of gold. $HAuCl_4 \cdot 4H_2O$ (99.9%, Au 48.0%, Merck), isopropanol (Fluka, GC grade, $\geq$99.5%) and citric acid trisodium salt dihydrate (Acros, 99%) were used without any further treatment. The gold chloride solutions were prepared with triple-distilled water from a Milli-Q water purification system (resistance 15 MΩ) and stored in the dark to avoid any further photoinduced decomposition. The synthesis of the ZnO/MWCNT composite is described elsewhere in the literature.[14]

Synthesis of Au/MWCNT and Au/ZnO/MWCNT composites: For the synthesis of the composite materials, acid-treated and untreated ZnO/MWCNT composites (400–500 mg) were impregnated overnight in a 2 mM aqueous solution of gold chloride (200 mL). Au deposition on the MWCNTs was carried out by two methods: 1) by reduction with sodium citrate and 2) by UV-light reduction using ZnO nanoparticles as the photoelectron donor and isopropanol as the hole acceptor. In Method 1, the gold chloride impregnated nanotubes were treated with sodium citrate (38.8 mmol) at 60 °C for approximately 18 h.[34] In Method 2, gold chloride was impregnated on MWCNTs in isopropanol (50 mL).[22] The photoreduction to gold was performed by placing the reaction mixture in a UV chamber (Hoenle UV technology, UVACUBE 2000) at a UV power of 160 mW cm^{-2} and a wavelength of $<$350 nm for 10 min. After the reaction, the initially pale yellow solution turned colourless indicating a quantitative reaction. The photodeposition of Au on the ZnO/MWCNT composite[14] was carried out in the same way as that used for the preparation of Au on the MWCNTs. The final products were filtered and washed with Millipore water until they were chloride free and were then dried at 100 °C overnight.

Table 1. Results of citral hydrogenation with Au/MWCNT and Au/ZnO/MWCNT composites as catalysts.[a]

Samples	Reduction method	Au content [wt%]	d_{Au} [nm][b]	Au shape	Citral conv. [%][c]	Selectivity (20% conversion)		
						UOL	CAL	Others[d]
MWCNT	–	–	–	–	33	8	13	79
Au/MWCNT	citrate	2.3	10–24	spherical	51	32	55	13
Au/MWCNT	UV light	2.8	2–8	irregular	39	15	20	65
Au/ZnO/MWCNT	UV light	2.3	3±1.5	single crystalline, hexagonal	28	50	33	17

[a] T=160 °C, $p(H_2)$=70 bar, solvent: n-hexane, m_{cat}=400 mg, V_{citral}=10 mL, $V_{n\text{-hexane}}$=90 mL, $V_{tetradecane}$=5 mL (internal standard for GC analysis). [b] Au particle size. [c] Conversion after 360 min. [d] Citronellol, 3,7-dimethyloctanol, isopulegol, non-identified products.

Sample characterisation: UV/Vis measurements were performed on suspensions of the products in ethanol against pure ethanol with a UV/Vis/NIR spectrometer (Lambda 900, Perkin–Elmer). Each sample was scanned in the range 280–800 nm. Micro-Raman measurements were carried out on a LabRAM HR high-resolution microscope from Horiba Jobin Yvon (model HR 800). The excitation wavelength used was 488 nm. The spectrum was recorded in the range of 50–4000 cm^{-1} for all of the nanocomposite materials. The gold content of the specimens was analysed by inductively coupled plasma optical emission spectrometry (ICP OES) using a Perkin–Elmer Optima 3000. The samples were prepared by dissolving a known amount of the nanocomposite in aqua regia. XRD of the samples was performed using a StadiP instrument (StadiP, Stoe and Cie GmbH, Darmstadt) in Debye–Scherrer mode (flat specimen, transmission mode) with $Cu_{K\alpha 1}$ radiation with a Ge(111) monochromator. XPS measurements were performed using an ESCA lab 250 instrument (thermo VG scientific) with monochromated $Al_{K\alpha}$ radiation in constant analyser energy mode (CAE) with a pass energy of 50 eV for all spectra. SEM investigations were performed with a Philips XL 30 FEG microscope at 20 keV. HRTEM investigations were carried out using a CM20FEG microscope (Philips) at 200 kV to determine the size and morphology of the gold particles. Samples were prepared in high purity ethanol and dripped on lacy-carbon copper grids. BET surface-area measurements were carried out with a Nova 3000e instrument. Surface area and sample pore size were analysed by using the nitrogen-sorption method.

Catalytic testing: Liquid-phase hydrogenation of citral was performed in a batch autoclave reactor (Parr Co.). The catalyst (400 mg) was mixed with *n*-tetradecane (5 mL; internal standard for GC analysis), citral (10 mL) and *n*-hexane (90 mL; as solvent). The reactor consisted of a chemically resistant Teflon vessel maintained at 160 °C. The hydrogenation was carried out under strict exclusion of oxygen by flushing the reactor with argon at 9 bar before the start of the experiment with at a stirring rate of 1200 rpm. The heating of the reaction mixture was also carried under argon, wherein the pressure increased to 15 bar. After reaching the required temperature, the batch reactor was pressurised with H_2 (70 bar) to start the hydrogenation reaction. Samples were taken periodically and analysed with off-line GC (instrument: HP 6890, DB-WAX).

Acknowledgements

Our work was supported through the Deutsche Forschungsgemeinschaft (DFG). We acknowledge Dr. Emanuel Ionescu (Raman spectra), Dr. Kathrin Hoffmann (XRD), MSc. Ravi Joshi (TEM) for technical assistance with the measurements and Prof. W. Jaegermann for making XPS studies possible. TEM studies were done under the project ERC-TUD-001 at Ernst-Ruska-Zentrum, Jülich (Prof. H. Meyer, Dr. L. Houben, Dr. A. Lysberg).

[1] S. Iijima, *Nature* **1991**, *354*, 56–58.
[2] a) A. C. Dillon, K. M. Jones, T. A. Bekkedahl, C. H. Kiang, D. S. Bethune, M. J. Heben, *Nature* **1997**, *386*, 377–379; b) R. H. Baughman, A. A. Zakhidov, W. A. de Heer, *Science* **2002**, *297*, 787–792.
[3] a) J. Li, Y. Lu, Q. Ye, M. Cinke, J. Han, M. Meyyappan, *Nano Lett.* **2003**, *3*, 929–933; b) N. Sinha, J. T. W. Yeow, *IEEE Nanobioscience* **2005**, *4*, 180–195; S. Sotiropoulou, N. A. Chaniotakis, *Anal. Bioanal. Chem.* **2003**, *375*, 103–105.
[4] a) B. Gao, A. Kleinhammes, X. P. Tang, C. Bower, L. Fleming, Y. Wu, O. Zhou, *Chem. Phys. Lett.* **1999**, *307*, 153–157; b) H. Shimoda, B. Gao, X. P. Tang, A. Kleinhammes, L. Fleming, Y. Wu, O. Zhou, *Phys. Rev. Lett.* **2001**, *88*, 015502-1-4; c) G. Maurin, Ch. Bousqueta, F. Henn, P. Bernier, R. Almairac, B. Simon, *Chem. Phys. Lett.* **1999**, *312*, 14–18.
[5] P. Serp, M. Corrias, P. Kalck, *Appl. Catal. A* **2003**, *253*, 337–358.
[6] a) C. A. Dyke, J. M. Tour, *Chem. Eur. J.* **2004**, *10*, 812–817; b) N. Tagmatarchis, M. Prato, *J. Mater. Chem.* **2004**, *14*, 437–439; c) M. Aizawa, M. S. P. Shaffer, *Chem. Phys. Lett.* **2003**, *368*, 121–124; d) A. Hirsch, *Angew. Chem.* **2002**, *114*, 1933–1939; *Angew. Chem. Int. Ed.* **2002**, *41*, 1853–1859.
[7] a) A. G. Rinzler, J. Liu, H. Dai, P. Nikolaev, C. B. Huffman, F. J. Rodriguez-Macias, B. J. Boul, A. H. Lu, D. Heymann, D. T. Colbert, R. S. Lee, J. E. Fischer, A. M. Rao, P. C. Eklund, R. E. Smalley, *Appl. Phys. A* **1998**, *67*, 29–37; b) H. Kuzmany, A. Kukovecz, F. Simon, M. Holzweber, Ch. Kramberger, T. Pichler, *Synth. Met.* **2004**, *141*, 113–122; c) S. Musso, S. Porro, M. Vinante, L. Vanzetti, R. Ploeger, M. Giorcelli, B. Possetti, F. Trotta, C. Pederzolli, A. Tagliaferro, *Diamond Relat. Mater.* **2007**, *16*, 1183–1187.
[8] a) L. Jiang, L. Gao, *Carbon* **2003**, *41*, 2923–2929; b) A. Fasi, I. Palinko, J. W. Seo, Z. Konya, K. Hernadi, I. Kiricsi, *Chem. Phys. Lett.* **2003**, *372*, 848–852; c) B. Xue, P. Chen, Q. Hong, J. Lin, K. L. Tan, *J. Mater. Chem.* **2001**, *11*, 2378–2381; d) A. Chu, J. Cook, R. J. R. Heesom, J. L. Hutchison, M. L. H. Green, J. Sloan, *Chem. Mater.* **1996**, *8*, 2751–2754.
[9] a) B. C. Satishkumar, A. Govindraj, J. Mofokeng, G. N. Subbanna, C. N. R. Rao, *J. Phys. B* **1996**, *29*, 4925–4934; b) L. Qu, L. Dai, E. Osawa, *J. Am. Chem. Soc.* **2006**, *128*, 5523–5532.
[10] a) E. H. Espinosa, R. Ionescu, B. Chambon, G. Bedis, E. Sotter, C. Bittercourt, A. Felten, J. J. Pireaux, X. Correig, E. Llobet, *Sens. Actuators B* **2007**, *127*, 137–142; b) X. Wang, B. Xia, X. Zhu, J. Chen, S. Qiu, J. Li, *J. Solid State Chem.* **2008**, *181*, 822–827; c) S. W. Lee, W. M. Sigmund, *Chem. Commun.* **2003**, 780–781.
[11] a) J. H. Shi, Y. J. Qin, W. Wu, X. L. Li, Z. X. Guo, D. B. Zhu, *Carbon* **2004**, *42*, 455–458; b) S. Ravindran, K. N. Bozhilov, C. S. Ozkan, *Carbon* **2004**, *42*, 1537–1542; c) Y. Liu, L. Gao, J. Sun, *J. Phys. Chem. C* **2007**, *111*, 1223–1229.
[12] L. Cao, F. Scheiba, C. Roth, F. Schweiger, C. Cremers, U. Stimming, H. Fuess, L. Chen, W. Zhu, X. Qiu, *Angew. Chem.* **2006**, *118*, 5441–5445; *Angew. Chem. Int. Ed.* **2006**, *45*, 5315–5319.
[13] S. Guo, S. Dong, E. Wang, *J. Phys. Chem. A* **2008**, *112*, 8561–8568.
[14] J. Khanderi, R. C. Hoffmann, A. Gurlo, J. J. Schneider, *J. Mater. Chem.* **2009**, *19*, 5039–5046.
[15] T. Y. Shin, S. H. Yoo, S. Park, *Chem. Mater.* **2008**, *20*, 5682–5686.
[16] J. Radnik, C. Mohr, P. Claus, *Phys. Chem. Chem. Phys* **2003**, *5*, 172–177.
[17] C. Mohr, H. Hofmeister, J. Radnik, P. Claus, *J. Am. Chem. Soc.* **2003**, *125*, 1905–1911.
[18] G. C. Bond, C. Louis, D. T. Thompson in *Catalysis by Gold*, Catalytic Science Series, Vol. 6 (Eds.: G. J. Hutchings), Imperial College Press, London, **2006**.
[19] a) P. Claus, *Appl. Catal. A* **2005**, *291*, 222–229; b) P. Claus, H. Hofmeister, C. Mohr, *Gold Bull.* **2004**, *37*, 181–186.
[20] S. Schimpf, M. Lucas, C. Mohr, U. Rodemerck, A. Brückner, J. Radnik, H. Hofmeister, P. Claus, *Catal. Today* **2002**, *72*, 63–78.
[21] a) C. Milone, C. Crisafulli, R. Ingoglia, L. Schipilliti, S. Galvagno, *Catal. Today* **2007**, *122*, 341–351; b) C. Milone, R. Ingoglia, A. Pistone, G. Neri, F. Frusteri, S. Galvagno, *J. Catal.* **2004**, *222*, 348–356; c) C. Milone, R. Ingoglia, M. L. Tropeano, G. Neri, S. Galvgno, *Chem. Commun.* **2002**, 868–869.
[22] J. Fernandez, A. Caballero, A. R. Gonzalez-Elipe, J. M. Herrmann, H. Dexpert, F. Villain, *J. Phys. Chem.* **1995**, *99*, 3303–3309.
[23] a) J. J. Schneider, R. C. Hoffmann, J. Engstler, O. Soffke, A. Issanin, A. Klyszcz, *Adv. Mater.* **2008**, *20*, 3383–3387; b) M. R. Hill, A. W. Jones, J. J. Russel, N. K. Roberts, R. N. Lamb, *Inorg. Chim. Acta* **2005**, *358*, 201–206.
[24] M. A. Correa-Duarte, N. Sobal, L. M. Liz-Marzan, M. Giersig, *Adv. Mater.* **2004**, *16*, 2179–2184; M. A. Correa-Duarte, J. Pérez-Juste, A. Sánchez-Iglesias, M. Giersig, L. M. Marzán, *Angew. Chem.* **2005**, *117*, 4449–4452; *Angew. Chem. Int. Ed.* **2005**, *44*, 4375–4378.
[25] N. S. Phala, G. Klatt, E. van Steen, S. A. French, A. A. Sokol, C. R. A. Catlow, *Phys. Chem. Chem. Phys.* **2005**, *7*, 2440–2445.
[26] H. Murphy, P. Papakonstantinou, T. I. T. Okpalugo, *J. Vac. Sci. Technol. B* **2006**, *24*, 715–720.
[27] K. Mcguire, Z. W. Pan, Z. L. Wang, D. Milkie, J. Menendez, A. M. Rao, *J. Nanosci. Nanotechnol.* **2002**, *2*, 499–502.

[28] R. Y. Sato-Berrú, A. Vazquez-Olmos, A. L. Fernandez-Osorio, S. Sotres-Martinez, *J. Raman Spectrosc.* **2007**, *38*, 1073–1076.
[29] D. W. Langer, C. J. Vesely, *Phys. Rev. B* **1970**, *2*, 4885–4892.
[30] M. S. Bhuvaneswari, N. N. Bramnik, D. Ensling, H. Ehrenberg, W. Jaegermann, *J. Power Sources* **2008**, *180*, 553–560.
[31] T. I. T. Okpalugo, P. Papakonstantinou, H. Murphy, J. McLaughlin, N. M. D. Brown, *Carbon* **2005**, *43*, 153–161.
[32] J. Yu, N. Grossiord, C. E. Koning, J. Loos, *Carbon* **2007**, *45*, 618–623.
[33] C. Mohr, H. Hofmeister, P. Claus, *J. Catal.* **2003**, *213*, 86–94.
[34] A. D. Mcfarland, C. L. Haynes, C. A. Mirkin, R. P. Van Duyne, *J. Chem. Educ.* **2004**, *81*, 544A–544B.

Received: July 17, 2009
Published online: December 22, 2009

